

# Engineered ultraviolet InGaN/AlGaIn multiple-quantum-well structures for maximizing cathodoluminescence efficiency

Cite as: AIP Advances 12, 015005 (2022); <https://doi.org/10.1063/6.0001262>

Submitted: 12 August 2021 • Accepted: 26 November 2021 • Published Online: 04 January 2022

Haiyang Zheng,  Vijay Kumar Sharma, Pingchieh Tsai, et al.



View Online



Export Citation



CrossMark

## ARTICLES YOU MAY BE INTERESTED IN

[Experimental study of the dispersion of cough-generated droplets from a person going up- or downstairs](#)

AIP Advances 12, 015002 (2022); <https://doi.org/10.1063/5.0073880>

[Numerical simulation of breakdown properties and streamer development processes in SF<sub>6</sub>/CO<sub>2</sub> mixed gas](#)

AIP Advances 12, 015003 (2022); <https://doi.org/10.1063/5.0076343>

[Control of the chirality of a vortex in a ferroelectric nanodot by uniform electric fields mediated by inhomogeneous surface screening](#)

AIP Advances 12, 015001 (2022); <https://doi.org/10.1063/5.0076281>

READ NOW!

AIP Advances

Photonics and Optics Collection

# Engineered ultraviolet InGaN/AlGaIn multiple-quantum-well structures for maximizing cathodoluminescence efficiency

Cite as: AIP Advances 12, 015005 (2022); doi: 10.1063/6.0001262

Submitted: 12 August 2021 • Accepted: 26 November 2021 •

Published Online: 4 January 2022



View Online



Export Citation



CrossMark

Haiyang Zheng,<sup>1</sup> Vijay Kumar Sharma,<sup>1,2</sup>  Pingchieh Tsai,<sup>1</sup> Yiping Zhang,<sup>1</sup> Shunpeng Lu,<sup>1</sup> Xueliang Zhang,<sup>1</sup> Swee Tiam Tan,<sup>1,3,a)</sup>  and Hilmi Volkan Demir<sup>1,2,b)</sup> 

## AFFILIATIONS

<sup>1</sup>School of Electrical and Electronic Engineering, School of Physical and Mathematical Sciences, LUMINOUS! Center of Excellence for Semiconductor Lighting and Displays, Nanyang Technological University, Singapore 639798, Singapore

<sup>2</sup>Department of Electrical and Electronics Engineering, Department of Physics, and UNAM–Institute of Materials Science and Nanotechnology, Bilkent University, TR 06800 Ankara, Turkey

<sup>3</sup>School of Energy and Chemical Engineering, Xiamen University Malaysia, Jalan Sunsuria, Bandar Sunsuria, 43900 Sepang, Selangor, Malaysia

<sup>a)</sup>Electronic mail: [sweetiam.tan@xmu.edu.my](mailto:sweetiam.tan@xmu.edu.my)

<sup>b)</sup>Author to whom correspondence should be addressed: [hvdemir@ntu.edu.sg](mailto:hvdemir@ntu.edu.sg)

## ABSTRACT

We demonstrate a systematic way to understand and select the accelerating voltage for maximizing cathodoluminescence (CL) by correlating the carrier diffusion length with the efficiency of ultraviolet (UV) InGaN/AlGaIn multiple quantum wells (MQWs). We showed that the absorption of MQWs benefits from the absorbed energy within the diffusion length below the MQWs. With this understanding, we have achieved good agreement between the experimental data of and the Monte Carlo (CASINO) simulations on the dependence of acceleration voltage and QW number on InGaN/AlGaIn MQW structures. These findings indicate that CL-based UV generation from carefully engineered III-N MQW structures with an appropriate number of QWs is highly promising. The understanding and application of this work can be extended to electron-beam pumped devices emitting in deep-UV (200–280 nm) wavelengths.

© 2022 Author(s). All article content, except where otherwise noted, is licensed under a Creative Commons Attribution (CC BY) license (<http://creativecommons.org/licenses/by/4.0/>). <https://doi.org/10.1063/6.0001262>

## I. INTRODUCTION

Ultraviolet (UV) AlGaIn-based light-emitting diodes (LEDs) are emerging as a potential substitute to conventional toxic mercury light sources. Depending on their emission wavelength, AlGaIn devices can be used in a variety of applications, including industrial curing, currency detection, photocatalysis, disinfection, and sterilization.<sup>1</sup> With their emission wavelength in the deep-UV (DUV) range (220–280 nm), it is challenging to realize high-performance current-driven devices since p-doping and ohmic contact formation pose major technical challenges to be achieved at high Al concentrations.<sup>2,3</sup> An alternative approach that may bypass these difficulties is electron-beam pumping.

Cathodoluminescence (CL) from e-beam pumped AlGaIn multiple-quantum-wells (MQWs) has been reported previously.<sup>4–11</sup>

Although it is a common notion that the luminescence properties deteriorate by increasing the number of QWs in the MQW region, Hospodková *et al.*<sup>4,5</sup> reported that 30 QW structures have higher efficiency than the ten QW InGaIn/GaN MQW structures. A few other groups also reported the correlation between structural and optical properties of the QW number in InGaIn-based MQWs with a variety of results.<sup>7,12</sup> Tabataba-Vakili *et al.*<sup>9</sup> studied the CL properties of Al<sub>0.56</sub>Ga<sub>0.44</sub>N/Al<sub>0.9</sub>Ga<sub>0.1</sub>N MQW structure and found that electron beams with 12 keV beam energy and 4.4 mA beam current maximize the output power. Ivanov *et al.*<sup>13</sup> studied electron-beam pumped AlGaIn MQWs in both pulsed and continuous wave (CW)-modes, and they found that in both cases, the power efficiency (PE) is less than 0.24%. The maximum PE of ~0.2% was obtained at 16 keV because of the good match of the e-beam excitation depth with the thickness of the MQW region in the struc-

ture. Recently, Oto *et al.*<sup>10</sup> reported e-beam pumped AlGaN/AlN MQWs with a record 100 mW power DUV light source with a PE of ~40%, whereas most of the other researchers reported <1% PE with similar structures.<sup>14</sup> Oto *et al.*<sup>10</sup> attributed this record value to the carrier confinement within the high-quality quantum wells and the design of the sample structures. Although high-quality MQWs play a huge role in this difference, the physical mechanism behind such high power remains unclear. It is a common understanding that the e-beam depth and the MQW thickness should match for higher optical output.<sup>9,10,13</sup> We believe that besides matching, the e-beam depth, and MQW thickness, the diffusion length of the layer below the MQWs also plays an important role. To the best of our knowledge, there have been no previous reports in which the CL properties of InGaN/AlGaN MQWs were systematically investigated. Thus, in this work, we proposed and demonstrated a systematic way to understand and select the accelerating voltage for maximizing CL efficiency and explained the associated behavior by correlating the carrier diffusion length with the CL efficiency of ultraviolet (UVA) InGaN/AlGaN MQWs. This understanding can be further extended to the light-emitting sources in the DUV (200–280 nm) region, which is of great interest for disinfection related applications.

## II. EXPERIMENT

In this work, all the epitaxial wafers were grown on c-plane sapphire substrates by our AIXTRON close-coupled showerhead metal-organic chemical-vapor deposition (MOCVD) system. The epitaxial structure started with a 30 nm thick GaN buffer layer, followed by a 3  $\mu\text{m}$  thick unintentionally doped GaN (u-GaN) layer, and then a 3  $\mu\text{m}$  thick Si-doped *n*-type GaN (*n*-GaN) layer with a doping concentration of  $5 \times 10^{18} \text{ cm}^{-3}$ . Finally, several pairs of  $\text{In}_{0.03}\text{Ga}_{0.97}\text{N}/\text{Al}_{0.05}\text{Ga}_{0.95}\text{N}$  MQWs were grown with a 2 nm thick ( $d_w$ )  $\text{In}_{0.03}\text{Ga}_{0.97}\text{N}$  QW and a 7.3 nm thick ( $d_b$ )  $\text{Al}_{0.05}\text{Ga}_{0.95}\text{N}$  quantum barrier (QB). We comparatively investigated four MQW structures with  $n = 8, 10, 15,$  and  $20$  pairs of quantum well-barrier structures, and the schematic diagram of the epitaxial structure is shown in Fig. 1(a).

Figure 1(b) shows the experimental setup of our CL measurements inside the vacuum chamber (not shown). The samples were loaded in the vacuum chamber installed with an e-gun that produces a collimated e-beam. An optical fiber was placed in proximity behind the samples and connected to an Avantes spectrometer to record CL spectra (not shown). For the power measurements, we used a Thorlabs photodiode power sensor (S120VC) as shown in Fig. 1(b). A UV transparent filter glass was placed between the sample and the sensor to block visible light for the power measurements. After loading the sample (InGaN/AlGaN MQW epitaxial structure), the chamber was filled with vacuum to reach a vacuum level of  $\sim 5 \times 10^{-7}$  hPa. Subsequently, the samples were pumped by e-beams with a spot diameter of 1 cm.

It is also important to determine the optimal anode acceleration voltage and current to realize an efficient MQW structure. Electrons irradiated onto a solid penetrate the semiconductor and mutually interact with other electrons and atomic nuclei. Suppose the penetration depth is much greater than the thickness of the MQW region; in that case, some irradiated electrons may go through that region and recombine in the underlying GaN layer by degrading the efficiency. However, if the penetration depth is too narrow,

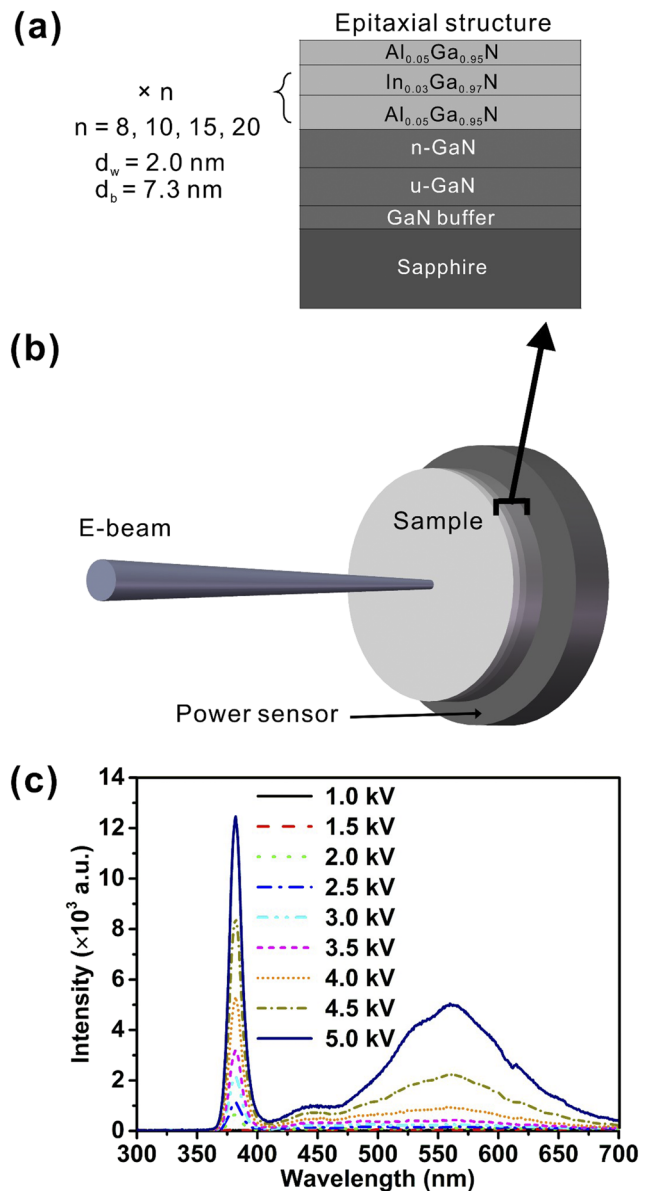


**FIG. 1.** (a) Schematic diagram of our grown InGaN/AlGaN MQW epitaxial structure. Here,  $d_w$ ,  $d_b$ , and  $n$  stand for the QW thickness, QB thickness, and QW number, respectively. (b) CL measurement setup inside the vacuum chamber and (c) CL spectra (recorded using Avantes spectrometer) parameterized to the acceleration voltage for the MQW structure with  $n = 8$  at a constant emission current of  $5 \mu\text{A}$ .

MQWs located away from the surface do not receive enough carriers. Therefore, to maximize the output power, the appropriate selection of anode voltage to match a given MQW structure is essential. To determine the optimum combination of MQW structure and anode voltage, we simulated numerous electron trajectories in our MQWs under different anode voltages using a Monte Carlo method (“CASINO” software).<sup>15</sup> In the software, we set the beam

radius to 10 nm and set up the whole epitaxial structure with known thickness. By varying the accelerating voltages, we obtained a cross-sectional view of absorbed energy in the epitaxial structure. Then we analyzed the CL intensity as a function of incident electron energy by quantitatively evaluating the absorbed energy at the MQW layer.

### III. RESULTS AND DISCUSSION

Figure 1(c) shows the CL spectra of our MQW structure with  $n = 8$  over a wide range of acceleration voltages at a constant emission current of  $5 \mu\text{A}$ . We observe a sharp UV peak at 380 nm and a broad peak from 450 to 700 nm centered at 560 nm. The sharp UV peak is attributed to the MQWs, and the broad peak is attributed to the defect band luminescence of GaN.<sup>4,5</sup> The CL intensity of the broad peak grows simultaneously with the UV peak initially as the beam energy increases and rises more rapidly after the acceleration voltage reaches 4 kV. This rapid increase in the defect-band CL intensity after 4 kV implies that the incident energetic electrons have penetrated into the deeper part below the MQWs.<sup>5</sup>

Figure 2(a) shows the measured normalized CL power efficiency (PE) as a function of the acceleration voltage at an emission current of  $50 \mu\text{A}$  for the MQW structures with  $n = 8, 10, 15,$  and  $20$ . Figure 2(b) shows the extracted maximum PE obtained at acceleration voltages as a function of the QW number. It is noted that the MQW structures with 8, 10, 15, and 20 pairs exhibit maximum PE levels of 0.27%, 0.29%, 0.23%, and 0.19% at an e-beam acceleration voltage of 9, 9, 10, and 13 kV, respectively.

In our case, we observed low efficiencies because we measured the light output from the sapphire side (most of the light is absorbed by GaN as can be seen from Fig. 1). Nevertheless, the measurement results are comparable since the measurements were carried out the same way. The PE can be improved by increasing the QW number from 8 to 10, but further increasing the QW number will result in efficiency deterioration. In our previous work,<sup>16</sup> we have compared the carrier-lifetime of LEDs with 3, 5, 8, and 11 QWs and found that considerable defects are generated in the case of 11 QWs because of misfit strain relaxation as we increase the thickness. Similar results were also reported by other research groups.<sup>17–19</sup> In our case, the MQW structure with ten QWs demonstrates the best efficiency, as can be seen from Fig. 2(b). Moreover, the e-beam acceleration voltage shifts from 9 to 13 kV when the QW number increases from 8 to 20. These observations suggest that there is a definitive correlation between the e-beam acceleration voltage and QW numbers. To substantiate this observation, we further simulated the electron trajectories in the MQWs as a function of the acceleration voltage using the Monte Carlo method.

Figure 3(a) shows absorbed energy simulated as a function of the e-beam acceleration for the InGaN/AlGaIn MQW structure with eight QWs using the Monte Carlo method. We observe that the absorbed energy reaches a maximum at 5 kV. To elucidate this absorption maximum, in Fig. 3(b), we plot the depth profiles of the cumulative absorbed energy starting from the top of MQWs at acceleration voltages of 3, 5, and 9 kV. The vertical dashed line marks the bottom of MQWs. The depth profiles reveal that most of the electron energy is absorbed in the MQWs when the acceleration voltage reaches 5 kV whereas smaller amounts of electron energy are absorbed in the MQWs with both higher and lower

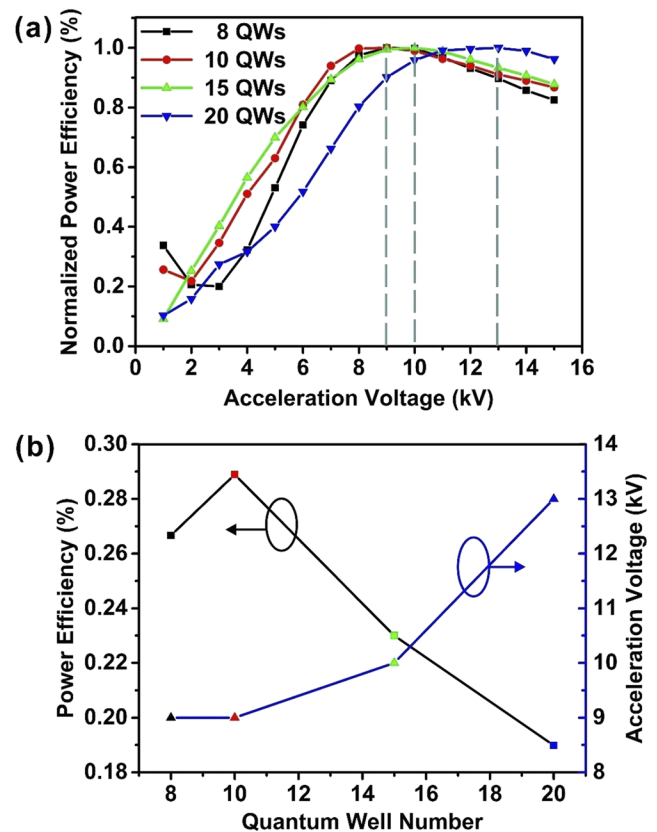


FIG. 2. (a) Normalized CL PE (recorded using Thorlabs photodiode power sensor) as a function of the acceleration voltage at an emission current of  $50 \mu\text{A}$  for different MQW structures and (b) maximum PE obtained at different acceleration voltages as a function of the QW number.

acceleration voltages. As we already know, the electrons penetrate deeper with higher acceleration voltage, and this suggests that if the electrons only reach the QWs closer to the surface, the other QWs will not receive sufficient electrons. However, if the electrons penetrate the MQWs, the electrons will go through the MQWs and will not be absorbed into the MQWs. Therefore, there is an optimum acceleration voltage (5 kV) that maximizes the absorbed energy, as shown in Fig. 3(b). It is a common understanding that CL intensity is directly proportional to the absorbed energy in MQWs.<sup>11</sup> Therefore, maximum absorbed energy corresponds to maximum PE. However, this simulation result shows a much lower acceleration voltage than the experimental value.

To understand this discrepancy between experiments and simulations, we used the concept of diffusion length. It is reasonable to assume that the carriers generated below the MQWs could diffuse back to the MQWs and contribute to the energy absorbed in the MQWs.<sup>9</sup> In other words, the electrons absorbed within the diffusion length below the MQWs generate free carriers, and these carriers will travel back and recombine in the MQWs. Therefore, we hypothesize that one needs to incorporate an added segment below the MQWs into the MQW region and combine both contributions. To confirm this hypothesis, we parameterized the contribution from

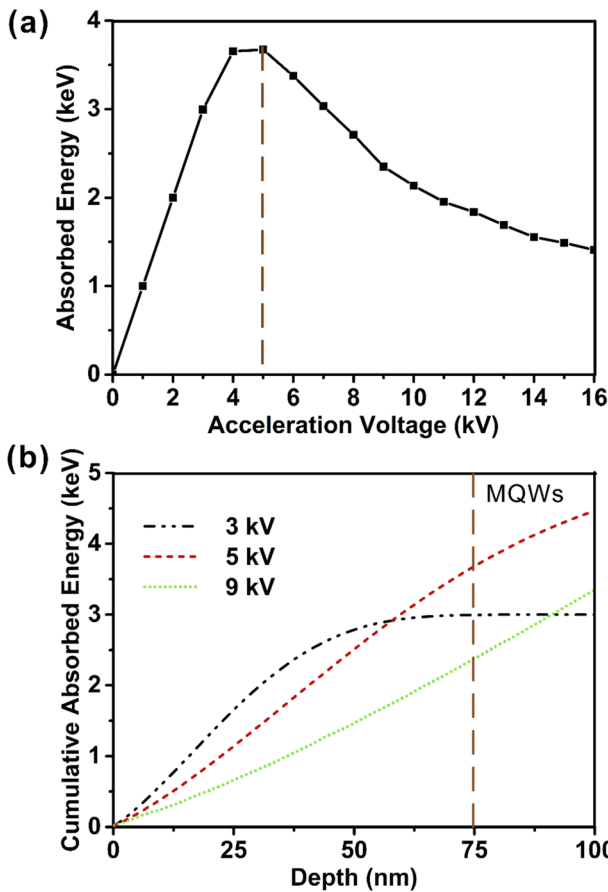


FIG. 3. (a) Absorbed energy simulated as a function of the acceleration voltage for the MQW structure with eight QWs and (b) simulated depth profiles of the cumulative absorbed energy from the MQW top (the vertical dashed line marks the bottom of MQWs).

the carrier diffusion from the region below the MQWs by repeating the simulations with varied diffusion lengths, and the results are presented in Fig. 4. As the diffusion length increases, the acceleration voltage shifts to a higher value, as visible from Fig. 4; if we use 160 nm diffusion length, the simulation predicts the same acceleration voltage as the experimental value. The typical diffusion length reported for *n*-GaN is in the range from 70 to 400 nm.<sup>20,21</sup> Among them, especially for *n*-GaN with a Si doping concentration of  $5 \times 10^{18} \text{ cm}^{-3}$ , the diffusion length reported is  $150 \pm 25 \text{ nm}$ .<sup>22</sup> Therefore, in our case, it is reasonable to use a 160 nm diffusion length in our simulations.

With this understanding, we studied the electron trajectories in the MQWs as a function of the acceleration voltage for InGaN/AlGaIn MQW structures with 8, 10, 15, and 20 QWs, and the simulation results are shown in Fig. 5(a). It is noted that the acceleration voltage shifts from 9 to 11 kV when the QW number increases from 8 to 20. The acceleration voltages extracted as a function of the QW number are shown in Fig. 5(b). In Fig. 5(b), we compared the experimental data shown in Fig. 2(b) with the simulated data, which

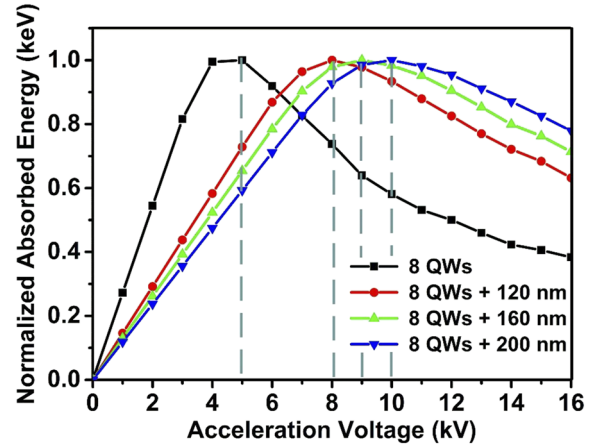


FIG. 4. Simulated normalized absorbed energy as a function of the acceleration voltage for the MQW structure with eight QWs with and without diffusion lengths (120, 160, and 200 nm).

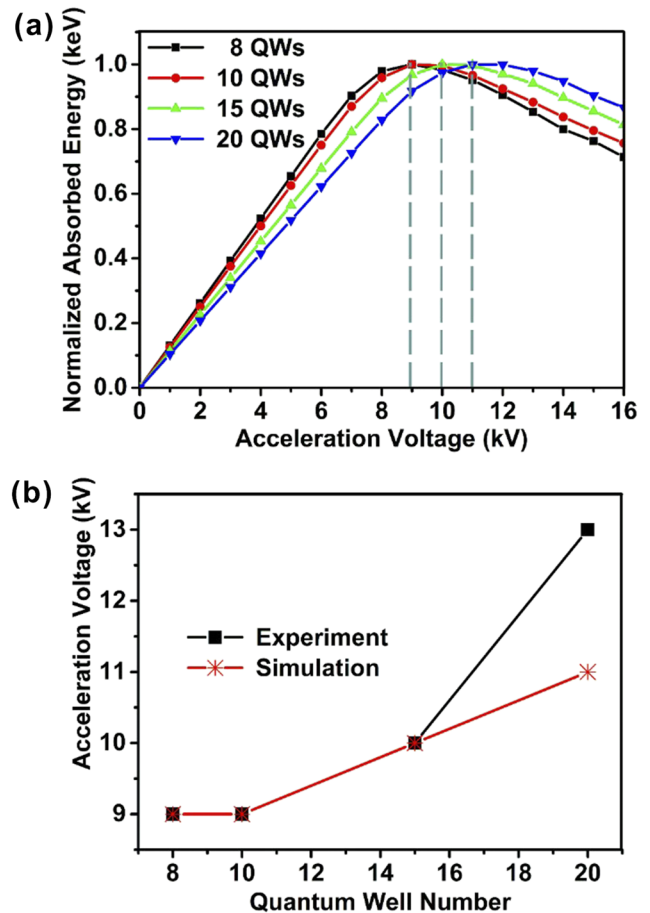


FIG. 5. (a) Absorbed energy simulated as a function of the acceleration voltage for the MQW structure with 8, 10, 15, and 20 QWs with a diffusion length of 160 nm and (b) comparison of experimental data for acceleration voltage as a function of the QW number with the simulated data.

shows good agreement in the dependence of the acceleration voltage on the QW number before it reaches 20. Similar to other research groups, we have also demonstrated in our previous work that the quality of the MQWs deteriorates when the QW number is increased beyond 10.<sup>16</sup>

#### IV. SUMMARY AND CONCLUSIONS

In summary, we have systematically studied and understood the CL characteristics of UVA InGaN/AlGaIn MQWs structures with 8, 10, 15, and 20 QWs and showed the acceleration voltage where the CL power efficiency is maximized. We observe that the acceleration voltage shifts from 9 to 13 kV when the QW number increases from 8 to 20. We established a relationship between the acceleration voltage and the QW number by introducing an additional contribution to MQW absorption from carriers generated within the diffusion length below the MQWs. In addition, we have also demonstrated that the MQW structure with ten QW pairs yields the best performance. This understanding provides insight into and guidelines for designing efficient CL-based devices and can be extended to DUV wavelengths.

#### ACKNOWLEDGMENTS

This research work was jointly supported by LightLab AB, Sweden, and NTU, Singapore.

#### AUTHOR DECLARATIONS

##### Conflict of Interest

The authors have no conflicts to disclose.

##### Author Contributions

H.Z. and V.K.S. contributed equally to this work. This article is a combined effort of all the authors.

#### DATA AVAILABILITY

The data that support the findings of this study are available from the corresponding author upon reasonable request.

#### REFERENCES

- <sup>1</sup>A. Khan, K. Balakrishnan, and T. Katona, *Nat. Photonics* **2**, 77 (2008).
- <sup>2</sup>Y. Taniyasu, M. Kasu, and T. Makimoto, *Nature* **441**, 325 (2006).
- <sup>3</sup>M. L. Nakarmi, N. Nepal, C. Ugolini, T. M. Altahtamouni, J. Y. Lin, and H. X. Jiang, *Appl. Phys. Lett.* **89**, 152120 (2006).
- <sup>4</sup>A. Hospodková, T. Hubáček, J. Oswald, J. Pangrác, K. Kuldová, M. Hývl, F. Dominec, G. Ledoux, and C. Dujardin, *Phys. Status Solidi B* **255**, 1700464 (2018).
- <sup>5</sup>A. Hospodková, J. Oswald, M. Zíková, J. Pangrác, K. Kuldová, K. Blazek, G. Ledoux, C. Dujardin, and M. Nikl, *J. Appl. Phys.* **121**, 214505 (2017).
- <sup>6</sup>T. Hubáček, A. Hospodková, K. Kuldová, J. Oswald, J. Pangrác, V. Jary, F. Dominec, M. Slavická Zíková, F. Hájek, E. Hulcius, A. Vetushka, G. Ledoux, C. Dujardin, and M. Nikl, *CrystEngComm* **21**, 356 (2019).
- <sup>7</sup>J. Yang, D. Zhao, D. Jiang, P. Chen, J. Zhu, Z. Liu, L. Le, X. He, X. Li, H. Wang, H. Yang, and U. Jahn, *J. Vac. Sci. Technol. A* **32**, 051503 (2014).
- <sup>8</sup>P. S. Vergeles, N. M. Schmidt, E. E. Yakimov, and E. B. Yakimov, *Phys. Status Solidi C* **8**, 1265 (2011).
- <sup>9</sup>F. Tabataba-Vakili, T. Wunderer, M. Kneissl, Z. Yang, M. Teepe, M. Batres, M. Feneberg, B. Vancil, and N. M. Johnson, *Appl. Phys. Lett.* **109**, 181105 (2016).
- <sup>10</sup>T. Oto, R. G. Banal, K. Kataoka, M. Funato, and Y. Kawakami, *Nat. Photonics* **4**, 767 (2010).
- <sup>11</sup>T. Matsumoto, S. Iwayama, T. Saito, Y. Kawakami, F. Kubo, and H. Amano, *Opt. Express* **20**, 24320 (2012).
- <sup>12</sup>F. C. P. Massabuau, L. Trinh-Xuan, D. Lodié, E. J. Thrush, D. Zhu, F. Oehler, T. Zhu, M. J. Kappers, C. J. Humphreys, and R. A. Oliver, *J. Appl. Phys.* **113**, 073505 (2013).
- <sup>13</sup>S. V. Ivanov, V. N. Jmerik, D. V. Nechaev, V. I. Kozlovsky, and M. D. Tiberi, *Phys. Status Solidi A* **212**, 1011 (2015).
- <sup>14</sup>D. Li, K. Jiang, X. Sun, and C. Guo, *Adv. Opt. Photonics* **10**, 43 (2018).
- <sup>15</sup>D. Drouin, A. R. Couture, D. Joly, X. Tastet, V. Aimez, and R. Gauvin, *Scanning* **29**, 92 (2007).
- <sup>16</sup>Y. P. Zhang, Z.-H. Zhang, W. Liu, S. T. Tan, Z. G. Ju, X. L. Zhang, Y. Ji, L. C. Wang, Z. Kyaw, N. Hasanov, B. B. Zhu, S. P. Lu, X. W. Sun, and H. V. Demir, *Opt. Express* **23**, A34 (2015).
- <sup>17</sup>M. Leyer, J. Stellmach, C. Meissner, M. Pristovsek, and M. Kneissl, *J. Cryst. Growth* **310**, 4913 (2008).
- <sup>18</sup>D. Holec, P. M. F. J. Costa, M. J. Kappers, and C. J. Humphreys, *J. Cryst. Growth* **303**, 314 (2007).
- <sup>19</sup>J. W. Matthews and A. E. Blakeslee, *J. Cryst. Growth* **27**, 118 (1974).
- <sup>20</sup>M. Hocker, P. Maier, L. Jerg, I. Tischer, G. Neusser, C. Kranz, M. Pristovsek, C. J. Humphreys, R. A. R. Leute, D. Heinz, O. Rettig, F. Scholz, and K. Thonke, *J. Appl. Phys.* **120**, 085703 (2016).
- <sup>21</sup>S. Hafiz, F. Zhang, M. Monavarian, V. Avrutin, H. Morkoç, Ü. Özgür, S. Metzner, F. Bertram, J. Christen, and B. Gil, *J. Appl. Phys.* **117**, 013106 (2015).
- <sup>22</sup>E. B. Yakimov, *J. Alloys Compd.* **627**, 344 (2015).